American Mineralogist, Volume 97, pages 2007–2015, 2012

Whelanite, $Cu_2Ca_6[Si_6O_{17}(OH)](CO_3)(OH)_3(H_2O)_2$, an (old) new mineral from the Bawana mine, Milford, Utah

Anthony R. Kampf,[1,*] Stuart J. Mills,[2] Stefano Merlino,[3] Marco Pasero,[3] Andrew M. McDonald,[4] William B. Wray,[5] and James R. Hindman[6]

[1]Mineral Sciences Department, Natural History Museum of Los Angeles County, 900 Exposition Boulevard, Los Angeles, California 90007, U.S.A.
[2]Geosciences, Museum Victoria, GPO Box 666, Melbourne 3001, Australia
[3]Dipartimento di Scienze della Terra, Università di Pisa, Via S. Maria 53, 56126 Pisa, Italy
[4]Department of Earth Sciences, Laurentian University, Sudbury, Ontario P3E 2C6, Canada
[5]2700 Las Vegas Boulevard South, no. 3310, Las Vegas, Nevada 89109, U.S.A.
[6]715 East Glendale Street, Dillon, Montana 59725, U.S.A.

Abstract

The new mineral whelanite, $Cu_2Ca_6[Si_6O_{17}(OH)](CO_3)(OH)_3(H_2O)_2$, was approved by the Commission on New Minerals and Mineral Names (IMA) in 1977, but until now a description has not been published. The mineral is orthorhombic with space group *Pn*2*n* and cell parameters $a = 5.6551(4)$, $b = 3.683(3)$, $c = 27.1372(7)$ Å, $V = 565.3(5)$ Å^3, and $Z = 1$. The mineral occurs with thaumasite, stringhamite, and kinoite in a copper-rich, diopside–garnet–magnetite skarn at the Bawana mine, Beaver County, Utah, and has also been confirmed to occur at other localities. At the Bawana mine, it is found as irregular clusters and radial aggregates of platy to lath-like crystals up to 1 mm in length, flattened on {001} and elongated on [100]. The color and streak are pale blue and the luster is vitreous. The laths are flexible, but not elastic. Cleavage is perfect on {001} and good on {010}, producing splintery fracture. The Mohs' hardness is about 2½. The measured density is 2.74(3) g/cm^3 and the calculated density is 2.737 g/cm^3 based upon the empirical formula. The mineral is biaxial (–), $\alpha = 1.612(2)$, $\beta = 1.622$(calc), and $\gamma = 1.626(2)$, and $2V_{meas} = 64(1)°$. The pleochroism is weak: X = Y (pale blue) < Z (light blue). The optical orientation is X = **a**, Y = **c**, Z = **b**. A combination of electron microprobe analyses and thermogravimetric analyses (for CO_2 and H_2O) yielded: CaO 34.46, CuO 12.09, FeO 1.52, SiO_2 37.96, CO_2 5.93, H_2O 8.86, total 100.82 wt%, providing the empirical formula (based on O = 26): $Cu_{1.41}Fe_{0.20}Ca_{5.68}Si_{5.84}C_{1.25}O_{26}H_{9.09}$. Raman spectroscopy shows evidence of $(CO_3)^{2-}$, $(OH)^-$, and H_2O. The strongest powder X-ray diffraction lines are [*d*(*hkl*)*I*]: 6.79(004)52, 3.072(111)43, 3.013(112)100, 2.921(113)39, 2.802(114)45, 2.522(116,205)44, and 1.839(020,1.1.12)37. The crystal structure (R_1 = 3.89% for 567 $F_o > 4\sigma F$) contains two different types of polyhedral layers parallel to {001}, which alternate along [001] and are linked to one another by sharing corners with wollastonite-like silicate chains running parallel [010]. One polyhedral layer, consisting of edge-sharing CaO_7 polyhedra, is identical to that in the structures of the tobermorites (tobermorite 9Å, tobermorite 11Å, tobermorite 14Å, and clinotobermorite). The other layer is brucite-like, with alternating ribbons of edge-sharing $Cu^{2+}O_6$ and CaO_6 octahedra. Disordered CO_3 and H_2O groups are also located in the interlayer region. The crystal structure of whelanite exhibits OD character.

Keywords: Whelanite, new mineral, crystal structure, order-disorder structure, Raman spectroscopy, Bawana mine, Milford, Utah

Introduction

The proposal for the new mineral whelanite (phonetically pronounced: WEE-lan-ite), submitted by one of the authors (J.R.H.), was approved by the Commission on New Minerals and Mineral Names (now known as the Commission on New Minerals, Nomenclature and Classification) of the International Mineralogical Association in 1977; however, until now, no formal description of the mineral has been published. A major stumbling block in investigations of the mineral has been the solution of its structure, which has proven quite elusive because of the thinness and generally poor quality of the vast majority of crystals, but more importantly, the disorder affecting the silicate-carbonate interlayer portion of the structure.

As indicated in the new mineral abstract, IMA 1977-006, type material is preserved in the Smithsonian Institution (U.S. National Museum of Natural History) and the Los Angeles County Museum of Natural History (now known as the Natural History Museum of Los Angeles County). The formal description of whelanite, provided herein, is based in part on data from the original study (density and TGA), but mostly on new data obtained from co-type material (10 specimens) in the Natural History Museum of Los Angeles County under catalog numbers 15507–15516.

* E-mail: akampf@nhm.org

0003-004X/12/1112–2007$05.00/DOI: http://dx.doi.org/10.2138/am.2012.4181

The mineral name honors the late James A. Whelan (1928–2003), who was a professor of mineralogy at the University of Utah, where he taught from 1958 to 1992.

Occurrence

The original specimens of whelanite were collected in 1969 at the Bawana (open pit) copper–magnetite mine, located about 5 miles NW of Milford in the Rocky mining district, Beaver County, Utah. The Bawana deposit, originally covered under several tens of feet of alluvium, was discovered by drilling a ground magnetic anomaly in late 1956, and was mined as an open pit from 1962 to 1967 (Wray 2006). A discussion of the geology and mineralogy of the area was provided by Hintze and Whelan (1973), and more recently by Wray (2006). We have also confirmed whelanite to occur on specimens from the Christmas mine, Pinal County, Arizona, and the Sunrise copper prospect near Bird Springs in the Nelson Range, Inyo County, California. A mineral from the Crestmore quarry, Riverside County, California, originally referred to by Murdoch (1961) as "mineral Y", appears to be closely related to whelanite. Numerous single-crystal samples of mineral Y that we examined provided powder X-ray diffraction patterns consistent with varying mixtures of whelanite and tobermorite 14Å, suggesting that the structure of this mineral may consist of interstratified whelanite and tobermorite 14Å layers.

At all of the localities whelanite is found as a late-stage phase in copper-rich, calc-silicate skarn assembages. At the Bawana mine, the mineral occurs with kinoite, stringhamite (Hindman 1976) and thaumasite on rock containing diopside, garnet (grossular–andradite), goethite, magnetite, and tenorite. Chrysocolla (including a blue copper-bearing silica gel) is abundant in the deposit and may occur on or near specimens containing whelanite and/or stringhamite. At the Christmas mine, whelanite occurs with gilalite, ruizite, stringhamite, and tobermorite 11Å on rock containing andradite, bornite, calcite, chalcopyrite, quartz, and wollastonite. At the Sunrise prospect, it occurs with apophyllite, lepidocrocite, stringhamite, and thaumasite on rock containing bornite, calcite, diopside, grossular, and tenorite. At the Crestmore quarry, the whelanite-like mineral occurs with foshagite, ganomalite, stringhamite, thaumasite, and tobermorite 14Å on rock containing calcite, galena, grossular, vesuvianite, and wollastonite.

The Rocky mining district contains other oxidized, near-surface copper–magnetite skarn deposits, several of which (the Maria, Hidden Treasure, and Hidden Treasure NW Extension deposits, in particular) have been mined. Despite efforts to locate whelanite in ore from these nearby, similar deposits, none has been found. Of possible significance is that these other deposits appear to lack the particular grossular–andradite host-rock association seen with the whelanite (and stringhamite) in the Bawana deposit. It is also noteworthy that mcguinnessite, which is similar in appearance to whelanite, occurs in small amounts as thin veinlets in massive magnetite in skarns of the Maria, Hidden Treasure, and Hidden Treasure NW Extension deposits, but has never been recognized in the Bawana deposit. Other oxidized copper-bearing skarn mines and deposits in the district, including among others the Old Hickory, Niagara, Sunrise, and Copper Ranch, are not known to contain any whelanite, stringhamite, or mcguinnessite.

After mining ceased at the Bawana mine, whelanite and associated stringhamite were only found within a small area of skarn rubble near the midpoint of the bottom of the open pit. Several decades of mineral collecting has depleted the occurrence, and recent excavation activity by a mining company has further disturbed the pit bottom, such that at the present time it is difficult or impossible to find specimens of these minerals.

Physical and optical properties

At the Bawana mine (and at the other localities), whelanite is found as irregular clusters and radial aggregates of platy to lath-like crystals (Figs. 1 and 2) up to 1 mm in length, flattened on {001} and elongated on [100]. Because of the thinness of the crystals, bounding forms could not be measured; however, based upon the shape of the laths, the {010} form accounts for the long edges of the laths and the terminations can be one of several {*hk*0} forms: {210}, {110}, {120}, or {130} (Fig. 3). The color and streak are pale blue and the luster is vitreous. The laths are flexible, but not elastic. Cleavage is perfect on {001} and good on {010}, producing splintery fracture. The Mohs hardness is about 2½. The measured density is 2.74(3) g/cm^3. The calculated density based upon the empirical formula and single-crystal cell is 2.738 g/cm^3 and that based upon the ideal formula is 2.856 g/cm^3.

Owing to the thinness of the plates, the β optical constant

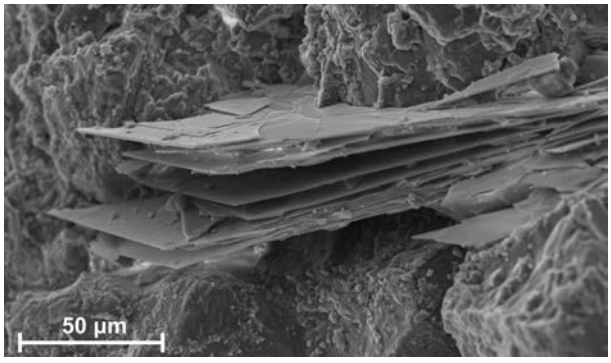

Figure 1. SEM image of whelanite from the Bawana mine.

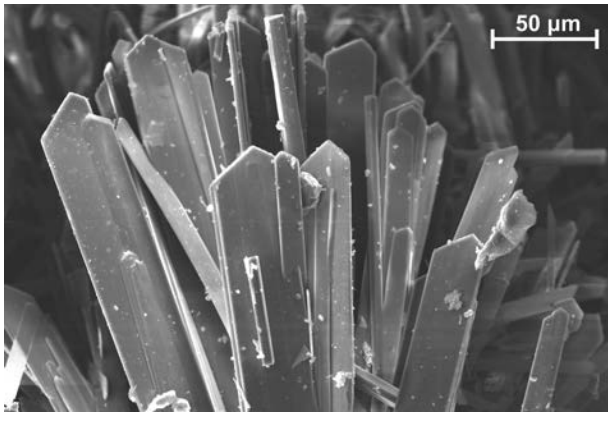

Figure 2. SEM image of whelanite from the Sunshine copper prospect.

could not be measured, and because of the unfavorable orientation, the interference figure could not be directly observed. Extinction data obtained on a Supper spindle stage were used with the program EXCALIBRW (Gunter et al. 2004) to determine the $2V$ angle. From the $2V$ and the measured indices of refraction α and γ, the value of β was calculated. All optical data were obtained in white light. Whelanite is optically biaxial (–) with optical constants: $\alpha = 1.612(2)$, $\beta = 1.622$(calc), and $\gamma = 1.626(2)$, and $2V_{meas} = 64(1)°$. The pleochroism is weak: $X = Y$ (pale blue) $< Z$ (light blue). The optical orientation is $X =$ **a**, $Y =$ **c**, $Z =$ **b**.

The Gladstone-Dale compatibility index $1 - (K_P/K_C)$, as defined by Mandarino (1981), is –0.037, indicating excellent agreement among the average index of refraction, calculated density, and chemical composition.

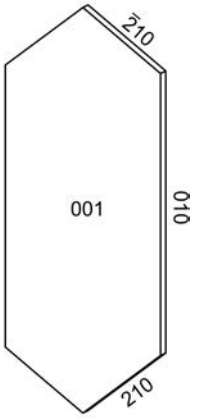

FIGURE 3. Crystal drawing of whelanite (clinographic projection in non-standard orientation).

RAMAN SPECTROSCOPY

Owing to questions regarding the chemical species present in whelanite, a Raman spectroscopic study was undertaken in this study. Subsequent to this, a published Raman spectrum of the mineral, obtained on non-type material from the Christmas mine, Gila Co., Arizona, was discovered (Frost and Xi 2012). Ignoring differences in band assignments and the number of peaks fit to some of the broader peaks, the two spectra are quite comparable in terms of the peaks present and their relative intensities. Given the similarity between the two spectra and that the current one was collected on type material, only the Raman spectrum from the Bawana mine (this study) is presented. The Raman spectrum (average of three, 30 s spectra) of a single crystal of whelanite was obtained over the range of 50 to 4000 cm^{-1} (Fig. 4). Data were collected in backscattered mode with a HORIBA Jobin Yvon XploRA spectrometer interfaced with an Olympus BX 41 microscope, 100× magnification (estimated spot size of 2 μm), a 1200 grating and an excitation radiation of 532 nm. Calibration was made using the 521 cm^{-1} line of Si from a silicon wafer. The Raman spectrum is dominated by a relatively sharp band at 671 cm^{-1} (weak shoulder at 715 cm^{-1}; attributable to asymmetrical Si-O bending, υ_4) that, along with several others below 1100 cm^{-1}, confirm the presence of SiO_4 in the mineral. The spectrum also shows strong peaks at 3558 cm^{-1} (shoulder at 3599 cm^{-1}) and 2954 cm^{-1} (shoulder at 2917 cm^{-1}) that can be

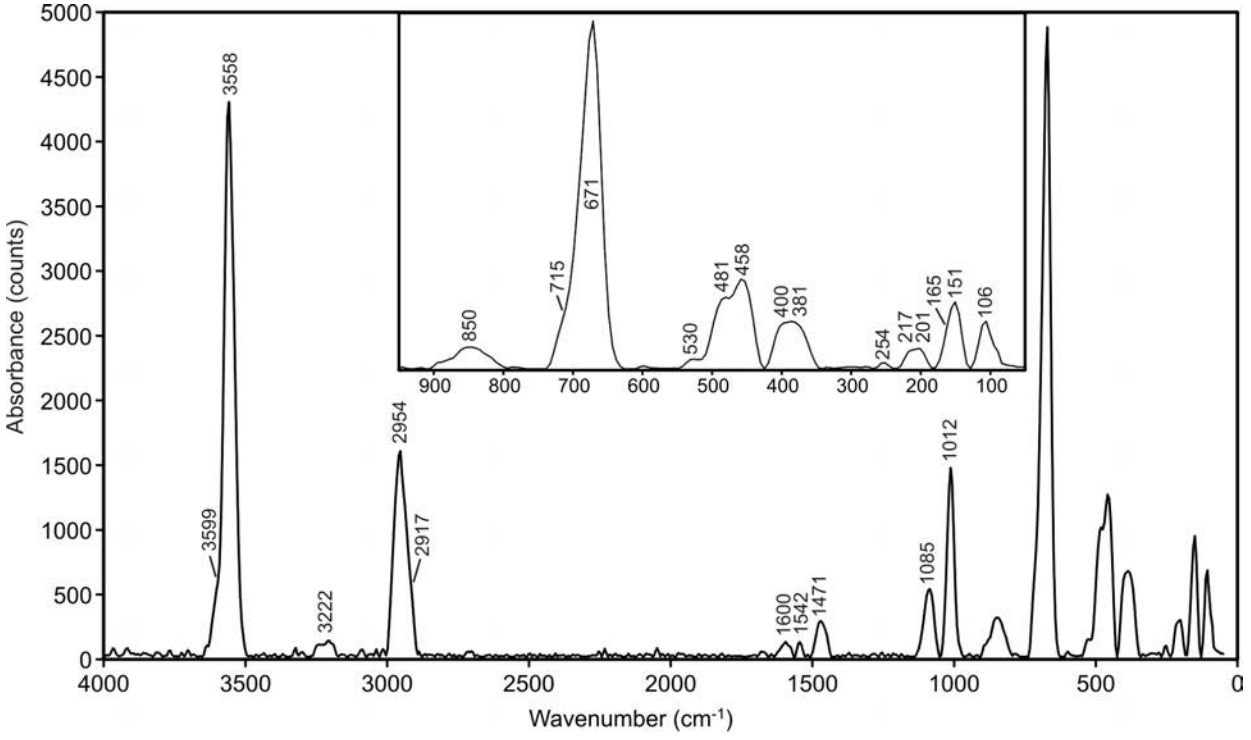

FIGURE 4. Raman spectrum for whelanite from 4000 to 50 cm^{-1}. Inset shows an expanded view of the region from 950 to 50 cm^{-1}. The absorption peaks are labeled with wavenumbers.

attributed to O-H stretching. Some Raman studies have argued that for multiple peaks in the region of 3000–3500 cm^{-1}, bands at relatively high frequencies are attributable to $(OH)^-$ and those at lower ones to H_2O [e.g., kovdorskite, $Mg_2PO_4(OH)\cdot 3H_2O$; Morrison et al. 2012]. In light of this, those bands near 3500 cm^{-1} could correspond to O-H stretching in $(OH)^-$ groups and those near 3000 cm^{-1} to that in H_2O groups. Thus the two sets of O-H stretching bands are taken as evidence that both species are present in whelanite. The region near 1500 cm^{-1} shows three weak absorption bands, two at 1600 and 1542 cm^{-1} that are attributable to H-O-H bending, thus implying the presence of molecular H_2O and one at 1471 cm^{-1}, attributable to C-O bending, thus confirming the presence of carbonate in the mineral. Table 1 lists all the observed absorption bands and the suggested assignments present in the Raman spectrum of whelanite. It should be noted that there is potential for overlap among several bands and these have been duly noted.

Chemistry

The original study of whelanite included chemical analyses utilizing various methods: electron microprobe (EMPA) for CaO, MgO, and CuO; wet chemical (WCA) for FeO and SiO_2; and thermogravimetric (TGA) for CO_2 and H_2O. In the present study, EMPA data for CaO, CuO, FeO, and SiO_2 (no other elements besides these having been detected) were collected by energy-dispersive spectrometry on a JEOL 6400 scanning electron microscope equipped with an Oxford Instruments INCA energy-dispersive spectrometer, operating at 20 kV with a 1 nA beam, and employing data collection times of 60 s. The system was first optimized for quantitative analyses using the Ni$K\alpha_1$ and Ni$K\alpha_2$ lines from metallic Ni, with chalcopyrite (Cu$K\alpha$, Fe$K\alpha$), quartz (Si$K\alpha$), and fluorite (Ca$K\alpha$) being used as internal standards. Results of the original TGA were used for CO_2 and H_2O. These combined data yield: CaO 34.46, CuO 12.09, FeO 1.52, SiO_2 37.96, CO_2 5.93, H_2O 8.86, total 100.82 wt%, providing the empirical formula (based on O = 26): $Cu_{1.41}Fe_{0.20}Ca_{5.68}Si_{5.84}C_{1.25}O_{26}H_{9.09}$. The ideal formula is $Cu_2Ca_6[Si_6O_{17}(OH)](CO_3)(OH)_3(H_2O)_2$, which requires CaO 34.61, CuO 16.36, SiO_2 37.08, CO_2 4.53, H_2O 7.41, total 100.00 wt%. As noted above, Raman spectroscopy confirms the presence of $(CO_3)^{2-}$ and suggests the presence of both $(OH)^-$ and H_2O.

Table 1. Observed absorption bands (cm^{-1}) and band assignments for the Raman spectrum of whelanite

Band	Strength	Suggested assignment
3599	m	Stretching mode of OH groups
3558	vs	Stretching mode of OH groups
3222	w	Stretching mode of OH groups
2954	s	Stretching mode of H_2O molecules
2917	m	Stretching mode of H_2O molecules
1600	w	H-O-H bend
1542	w	H-O-H bend/C-O Asymmetric stretching mode
1471	w	C-O Asymmetric stretching mode
1085	m	Si-O Asymmetric stretching mode/ C-O Symmetric stretching mode
1012	s	Si-O Asymmetric stretching mode
850	w	Si-O Symmetric stretching mode
715	w	Si-O Asymmetric bending mode/C-O Bending mode
671	vs	Si-O Asymmetric bending mode
530	w	Si-O Asymmetric bending mode
481	m	Si-O Symmetric bending mode
458	m	Si-O Symmetric bending mode
400	m	Cu-O, Ca-O stretching modes
381	m	Cu-O, Ca-O stretching modes
217	w	Lattice vibrations
201	w	Lattice vibrations
151	m	Lattice vibrations
106	m	Lattice vibrations

Note: vs = very strong, m = medium, w = weak.

X-ray crystallography and structure determination

Both powder and single-crystal X-ray diffraction data were obtained on a Rigaku R-Axis Rapid II curved imaging plate microdiffractometer utilizing monochromatized Mo$K\alpha$ radiation. For the powder-diffraction study, a Gandolfi-like motion on the φ and ω axes was used to randomize the sample and observed *d*-spacings and intensities were derived by profile fitting using JADE 2010 software. The powder data presented in Table 2 show good agreement with the pattern calculated from the structure determination.

Previous efforts to obtain single-crystal data had been plagued by severe streaking of diffraction spots due to the occurrence of crystals as fine-scale intergrowths of warped laths. A large number of crystal fragments were examined before one that provided single diffraction spots with minimal streaking was found. Even so, because of the extreme thinness (1 μm) of this blade, diffraction intensity fell off precipitously above 45 °2θ, limiting our data set.

The Rigaku CrystalClear software package was used for processing of the structure data including corrections for Lorentz and polarization effects and the application of an empirical multi-scan absorption correction using ABSCOR (Higashi 2001). The SHELXL-97 software (Sheldrick 2008) was used, with neutral atom scattering factors, for the determination (by direct methods) and refinement of the structure. The location of most atoms in the structure was straightforward in space group *Pn*2*n* with the cell: $a = 5.6551(4)$, $b = 3.683(3)$, and $c = 27.1372(7)$ Å; however, the Si2 site exhibited approximately half occupancy, the Si1 site was split into two sites, each with half occupancy, the geometries of the SiO_4 groups were highly irregular and no straightforward CO_3 group could be located. A variety of alternate unit cells with multiples of the cell dimensions were attempted, along with different space groups ranging even to *P*1, in an effort to establish reasonable SiO_4 (and CO_3) group geometries, but without positive results. We ultimately concluded that the irregular SiO_4 configurations are best explained by recourse to order-disorder (OD) theory, as explained below. The "missing" CO_3 group is not addressed in the OD analysis and we found no definitive evidence for its placement in the structure. In the discussion below, we conjecture on its possible placement; however, it should be noted here that the amount of CO_3 in the empirical formula would require a C site that is only about ¼ occupied, so it is not surprising that the CO_3 group is not clearly resolved in the difference maps.

The structure refinement, based upon the aforementioned space group and cell, represents the average structure. The two Ca sites (Ca1 and Ca2) refine to close to full occupancy, but the Cu site refines to somewhat less than full occupancy. All of the O sites associated with the Cu and Ca polyhedra (O1, O2, O3, O4, and O5) refine to close to full occupancy, while the O sites between the polyhedral layers (O6a, O6b, and O7)

TABLE 2. Observed and calculated X-ray powder-diffraction data for whelanite

I_{obs}	d_{obs}	d_{calc}	I_{calc}	*hkl*	I_{obs}	d_{obs}	d_{calc}	I_{calc}	*hkl*
52	6.79(4)	6.7843	74	0 0 4			2.0379	6	1.1.10
		5.5362	7	1 0 1	15	2.008(7)	2.0093	18	2 1 6
17	5.21(6)	5.2199	31	1 0 2	12	1.947(11)	1.9579	8	2.0.10
32	4.52(2)	4.5229	59	0 0 6			1.9413	8	2 1 7
18	3.65(5)	3.6495	13	0 1 1	10	1.874(7)	1.8709	18	2 1 8
7	3.53(3)	3.5321	21	1 0 6	37	1.839(6)	1.8415	35	0 2 0
28	3.40(5)	3.4111	11	0 1 3			1.8241	30	1.1.12
19	3.22(7)	3.1975	16	1 0 7	9	1.776(7)	1.7772	8	0 2 4
43	3.072(13)	3.0664	51	1 1 1			1.7661	8	2.0.12
100	3.013(16)	3.0093	100	1 1 2	12	1.728(18)	1.7288	12	2.1.10
39	2.921(14)	2.9209	41	1 1 3	8	1.703(19)	1.7056	7	0 2 6
		2.9090	14	1 0 8			1.6953	5	3 0 7
		2.8123	17	2 0 1	28	1.678(5)	1.6780	29	3 1 0
45	2.802(11)	2.8092	46	1 1 4	16	1.649(8)	1.6415	9	1.1.14
		2.7681	12	2 0 2	8	1.628(13)	1.6289	9	3 1 4
54	2.722(21)	2.7137	30	0.0.10	12	1.598(6)	1.5988	7	2.0.14
		2.6828	11	1 1 5			1.5984	8	3 0 9
		2.6607	10	1 0 9	5	1.572(15)	1.5732	5	3 1 6
11	2.609(18)	2.6099	19	2 0 4			1.5559	6	1 2 8
44	2.522(11)	2.5493	30	1 1 6	31	1.525(10)	1.5332	6	2 2 2
		2.5077	17	2 0 5			1.5238	12	0.2.10
		2.4466	6	1.0.10			1.5076	5	0.0.18
12	2.408(18)	2.3976	15	2 0 6			1.5047	5	2 2 4
8	2.333(11)	2.3331	16	0 1 9			1.4864	7	1.1.16
27	2.271(12)	2.2828	31	1 1 8	6	1.461(7)	1.4604	5	2 2 6
		2.2614	5	0.0.12			1.4545	5	2.0.16
		2.2612	5	1.0.11	9	1.427(8)	1.4272	9	3.1.10
13	2.16(9)	2.1719	11	2 0 8	16	1.405(7)	1.4062	9	4 0 2
		2.1567	6	1 1 9			1.4046	5	2 2 8
18	2.135(13)	2.1295	17	2 1 4					

Notes: I_{obs} and d_{obs} derived by profile fitting using JADE 2010 software. I_{calc} and d_{calc} calculated from the crystal structure using JADE 2010. Only calculated lines with intensities of 5 or greater are listed. Unit-cell parameters refined from the powder data using JADE 2010 with whole pattern fitting are: a = 5.6571(15), b = 3.6783(9), and c = 27.141(8) Å.

refine to close to half occupancy. Each of the Si sites (Si1a, Si1b, and Si2) also refine to about half occupancy. In the final refinement, all of the sites were assigned either full or half occupancy, as noted above, except the Cu site, for which the occupancy was refined. Note that the small amount of Fe detected in the chemical analysis does not account for the significant deficiency in scattering for the Cu site. We conclude that the low occupancy for this site reflects a real deficiency in Cu + Fe for the site, as also indicated by the lower than stoichiometric Cu + Fe total in the empirical formula. In the final refinement, we also employed the DFIX command to constrain the Si1a-O7 and Si1b-O7 distances to 1.63(2) Å to yield more normal Si-O bond lengths. We were unsuccessful in constraining the very long Si2-O4 bond (1.84 Å) to a more reasonable length and are forced to conclude that it is an artifact of the structural disorder. We were also unsuccessful in locating the CO_3 group indicated by the chemical analyses and Raman spectroscopy. No configurations of located O atoms and/or electron density residuals appear consistent with a CO_3 group.

The Flack parameter (Flack and Bernardinelli 1999), 0.37(12), indicated the likely presence of merohedral twinning and the TWIN instruction was included in the final refinement, which converged to R_1 = 3.89% for 567 reflections with $F_o > 4\sigma F$. The details of the data collection and structure refinement are provided in Table 3. The final atomic coordinates and displacement parameters are in Table 4. Selected interatomic distances and angles are listed in Table 5 and a bond-valence analysis is provided in Table 6. (CIF and structure factors on deposit[1].)

TABLE 3. Data collection and structure refinement details for whelanite

Diffractometer	Rigaku R-Axis Rapid II
X-ray radiation/power	Mo$K\alpha$ (λ = 0.71075 Å)/50 kV, 40 mA
Temperature	298(2) K
Structural formula (without C and H)	$Cu_{1.86}Ca_6Si_6O_{26}$
Space group	*Pn*2*n*
Unit-cell dimensions (Å)	a = 5.6551(4)
	b = 3.683(3)
	c = 27.1372(7)
Z	1
Volume (Å^3)	565.3(5)
Density (for structural formula) (g/cm^3)	2.771
Absorption coefficient (mm^{-1})	3.552
F(000)	465.9
Crystal size (μm)	150 × 50 × 1
θ range (°)	3.00 to 22.44
Index ranges	$-6 \le h \le 6$, $-3 \le k \le 3$, $-29 \le l \le 29$
Reflections collected/unique	3135/705 [R_{int} = 0.076]
Reflections with $F_o > 4\sigma F$	567
Completeness to θ = 23.25°	98.8%
Max. and min. transmission	0.9965 and 0.6178
Refinement method	Full-matrix least-squares on F^2
Parameters refined	89
GoF	1.069
Final R indices [$F_o > 4\sigma F$]	R_1 = 0.0389, wR_2 = 0.0818
R indices (all data)	R_1 = 0.0553, wR_2 = 0.0898
Flack parameter	0.37(12)
Largest difference peak/hole (e/A^3)	+0.99/–0.43

Notes: $R_{int} = \Sigma|F_o^2 - F_o^2(\text{mean})|/\Sigma[F_o^2]$. GoF = $S = \{\Sigma[w(F_o^2 - F_c^2)^2]/(n-p)\}^{1/2}$. $R_1 = \Sigma||F_o| - |F_c||/\Sigma|F_o|$. $wR_2 = \{\Sigma[w(F_o^2 - F_c^2)^2]/\Sigma[w(F_o^2)^2]\}^{1/2}$. $w = 1/[\sigma^2(F_o^2) + (aP)^2 + bP]$ where a is 0.0339, b is 2.0112, and P is $[2F_c^2 + \text{Max}(F_o^2,0)]/3$.

DISCUSSION OF THE STRUCTURE

General description of the structure

The structure of whelanite (Figs. 5a and 5b) contains two different types of polyhedral layers parallel to {001}, which alternate along [001] and are linked to one another by sharing corners with silicate groups in the layer region. One polyhedral layer, consisting of edge-sharing CaO_7 polyhedra, is identical to that in the structures of the tobermorites (tobermorite 9Å, tobermorite 11Å, tobermorite 14Å, and clinotobermorite). The other layer is brucite-like, with ribbons of edge-sharing Jahn-Teller distorted $Cu^{2+}O_6$ octahedra along [010] alternating with ribbons of edge-sharing CaO_6 octahedra (Fig. 6). The edge-sharing octahedral layer with alternating ribbons of $Cu^{2+}O_6$ and CaO_6 octahedra has not previously been reported in any mineral.

The linkage of the silicate groups is not immediately obvious because of the disorder manifest in this portion of the structure. An examination of the order-disorder (OD) character of the structure (see below) allowed us to rationalize the silicate region as consisting of two overlapping half-occupied wollastonite-like silicate chains running parallel [010] (Fig. 7). The chemical and Raman investigations indicate the presence of CO_3 and H_2O groups and these must presumably also be hosted in the interlayer region. We discuss their possible dispositions below.

The OD character of whelanite

OD theory was developed by Dornberger-Schiff (1956, 1964, 1966) to deal with order-disorder aspects and polytypic features

[1] Deposit item AM-12-081, CIF and structure factors. Deposit items are available two ways: For a paper copy contact the Business Office of the Mineralogical Society of America (see inside front cover of recent issue) for price information. For an electronic copy visit the MSA web site at http://www.minsocam.org, go to the *American Mineralogist* Contents, find the table of contents for the specific volume/issue wanted, and then click on the deposit link there.

in structures characterized by ambiguities in the stacking of adjacent structural layers. A recent account of OD theory may be found in Ferraris et al. (2008).

The average structure of whelanite, described above, was derived from the refinement using the "family reflections", i.e., those reflections related to the subcell (A = 5.655, B = 3.6835, C = 27.137 Å, and space group $Pn2n$).

The part of the real structure that may be derived from these data (subcell reflections) is formed by two modules corresponding to the two kinds of polyhedral layers: the tobermorite-like CaO_7 layer module and the $Cu^{2+}O_6$–CaO_6 octahedra layer module. These two modules in fact have repeat periods of A = 5.655 and B = 3.6835 Å in the (**a**,**b**) plane.

The structure of whelanite may be completed with the insertion of wollastonite chains between the above modules. The way in which the wollastonite chains are grasped to the tobermorite-like module is described in Merlino et al. (2000).

Adjacent wollastonite chains on the same side of the tobermorite-like module are shifted by **b**/2, whereas chains on the opposite sides of the module are shifted by ±**b**/4. In Figure 5c, the fractional height of the wollastonite chains is reported, with reference to the true periodicity along **b**, namely 7.367 Å.

The single OD layer (indicated in Fig. 5c by the square bracket) has layer group symmetry $C12(1)$, with translation vectors **a** and **b** (a = 11.310, b = 7.367 Å), and the third vector $\mathbf{c_0}$ (c_0 = 13.569 Å).

Among the possible OD groupoid families corresponding to the layer group $C12(1)$ (Dornberger-Schiff and Fichtner 1972;

TABLE 4. Fractional coordinates, occupancies and atom displacement parameters (Å²) for whelanite

	x	y	z	Occ.	U_{eq}	U_{11}	U_{22}	U_{33}	U_{23}	U_{13}	U_{12}
Cu	0.0000	0.0000	0.0000	0.920(7)	0.0161(6)	0.0084(8)	0.0238(9)	0.0160(9)	0.000	0.0012(6)	0.000
Ca1	0.5000	0.504(3)	0.0000	1	0.0166(6)	0.0145(11)	0.0161(13)	0.0192(13)	0.000	–0.0009(10)	0.000
Ca2	0.6498(2)	0.999(2)	0.78612(5)	1	0.0121(5)	0.0111(8)	0.0085(9)	0.0165(9)	–0.007(3)	–0.0005(7)	–0.003(3)
Si1a	0.650(2)	0.097(4)	0.6730(5)	0.50	0.0100(8)						
Si1b	0.652(2)	0.932(4)	0.6733(4)	0.50	0.0100(8)						
Si2	0.8015(7)	0.514(4)	0.59994(14)	0.50	0.0128(11)						
O1	0.3767(8)	0.501(5)	0.79316(17)	1	0.0124(11)	0.012(2)	0.014(3)	0.011(3)	0.006(9)	0.002(2)	0.005(9)
O2	0.9147(8)	0.498(5)	0.79607(18)	1	0.0165(12)	0.011(2)	0.015(3)	0.024(3)	0.005(12)	0.002(2)	–0.002(9)
O3	0.6983(8)	0.009(5)	0.03921(17)	1	0.0178(13)	0.015(3)	0.021(3)	0.018(3)	0.004(10)	0.002(2)	0.001(8)
O4	0.3914(13)	0.007(6)	0.1224(2)	1	0.051(2)	0.076(5)	0.054(5)	0.024(4)	–0.017(12)	–0.007(3)	0.002(14)
O5	0.1627(13)	0.668(3)	0.0440(3)	1	0.039(2)	0.020(4)	0.058(5)	0.039(5)	0.017(4)	–0.002(4)	0.004(4)
O6a	0.664(4)	0.843(7)	0.6234(8)	0.50	0.015(2)						
O6b	0.668(4)	0.132(6)	0.6184(8)	0.50	0.015(2)						
O7	0.6448(15)	0.511(5)	0.6515(3)	0.50	0.013(2)						

TABLE 5. Selected bond distances (Å) and angles (°) for whelanite

Cu-O5 (×2)	1.941(9)	Si1a-O2	1.614(14)	Si1b-O1	1.583(14)	Si2-O6a	1.57(3)
Cu-O3 (×2)	2.011(5)	Si1a-O1	1.616(14)	Si1b-O2	1.598(13)	Si2-O3	1.648(6)
Cu-O5 (×2)	2.886(10)	Si1a-O7	1.634(15)	Si1b-O7	1.660(15)	Si2-O6b	1.68(2)
<Cu-O>	2.279	Si1a-O6a	1.64(3)	Si1b-O6b	1.66(3)	Si2-O4	1.840(8)
		<Si1a-O>	1.63	<Si1b-O>	1.63	<Si2-O>	1.68
Ca1-O5 (×2)	2.331(8)						
Ca1-O3 (×2)	2.390(15)	O2-Si1a-O1	108.0(8)	O1-Si1b-O2	110.5(7)	O6a-Si2-O3	114.4(11)
Ca1-O3 (×2)	2.419(15)	O2-Si1a-O7	112.4(11)	O1-Si1b-O7	112.1(10)	O6a-Si2-O6b	107.7(5)
<Ca1-O>	2.380	O2-Si1a-O6a	109.8(12)	O1-Si1b-O6b	113.6(11)	O6a-Si2-O4	110.0(11)
		O1-Si1a-O7	114.8(10)	O2-Si1b-O7	107.9(11)	O3-Si2-O6b	106.8(11)
Ca2-O2	2.385(16)	O1-Si1a-O6a	107.7(12)	O2-Si1b-O6b	116.2(11)	O3-Si2-O4	109.3(3)
Ca2-O2	2.393(16)	O7-Si1a-O6a	103.8(12)	O7-Si1b-O6b	95.5(11)	O6b-Si2-O4	108.5(11)
Ca2-O1	2.406(13)	<O-Si1a-O>	109.4	<O-Si1a-O>	109.3	<O-Si1a-O>	109.5
Ca2-O1	2.417(14)						
Ca2-O4	2.495(8)						
Ca2-O1	2.505(5)						
Ca2-O2	2.597(5)						
<Ca2-O>	2.457						

TABLE 6. Bond valence sums for whelanite (values are expressed in valence units)

	Cu	Ca1	Ca2	Si1a	Si1b	Si2	Σ	Σ*
O1			0.31, 0.30 0.24	1.03 ×½→	1.12 ×½→		1.93	
O2			0.33, 0.32 0.18	1.02 ×½→	1.07 ×½→		1.88	
O3	0.41 × 2↓	0.32 × 2↓ 0.30 × 2↓				0.94	1.97	1.03
O4			0.24			0.56	0.80	0.24
O5	0.49 × 2↓ 0.04 × 2↓	0.38 × 2↓					0.91	
O6a				0.96		1.16	2.12	
O6b					0.91	0.86	1.77	
O7				0.97	0.91		1.88	
Σ	1.88	2.00	1.92	3.98	4.01	3.52		

Notes: Multiplicity is indicated by ×→↓. Cu^{2+}-O and Ca^{2+}-O bond strengths from Brown and Altermatt (1985). Si^{4+}-O bond strength from Brese and O'Keeffe (1991). The last column headed by Σ* indicates the bond-valence sums for O3 and O4 when they do not participate in bonding to Si2.

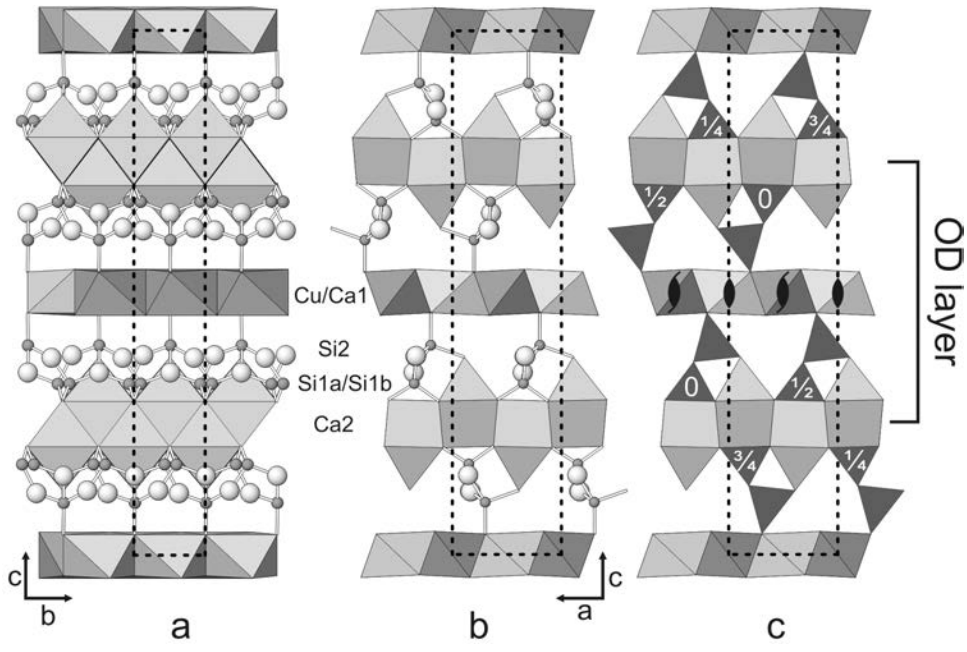

FIGURE 5. The crystal structure of whelanite (**a**) down [100], (**b**) down [010], and (**c**) down [010] showing OD features.

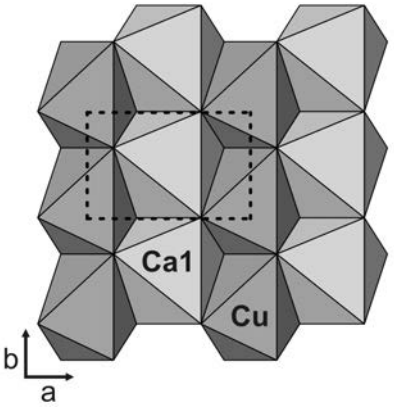

FIGURE 6. The brucite-like edge-sharing layer of octahedra in the structure of whelanite viewed down [001].

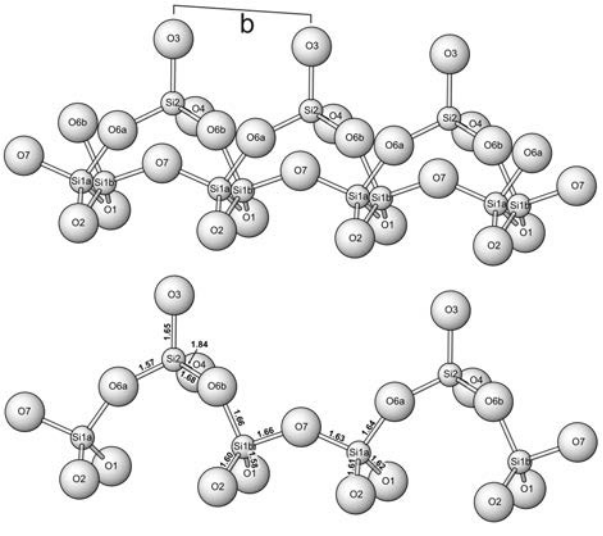

FIGURE 7. The overlapping, half-occupied, wollastonite-like silicate chains in whelanite (**top**) and only one of the chains (**bottom**); clinographic projection viewed approximately down [100]. The unit cell repeat along the **b**-axis is shown.

Ferraris et al. 2008), we found

$$\begin{matrix} C & 1 & 2 & (1) \\ \{ & n_{1/2,2} & 1\,(n_{1/2,1/2}) & \} \end{matrix} \qquad (1)$$

whose partial operations are compatible with the symmetry (*Pn*2*n*) of the family structure, which has the following basic vectors: $\mathbf{A} = \mathbf{a}/2$, $\mathbf{B} = \mathbf{b}/2$, and $\mathbf{C} = 2\mathbf{c}_0$.

The symbol (1) indicates that layers with symmetry *C* 1 2 1 may follow each other in the **c** direction, related by the operators $n_{1/2,2}$ (or $n_{-1/2,2}$) normal to **a** [and $n_{1/2,1/2}$ (or $n_{1/2,-1/2}$) normal to **c**].

There are two maximum degree of order (MDO) polytypes in this family: MDO1, corresponding to the sequence of OD layers in which the operators $n_{1/2,1/2}$ and $n_{1/2,-1/2}$ normal to **c** regularly alternate, and MDO2, corresponding to the sequence of layers in which the operator $n_{1/2,1/2}$ is constantly applied (the constant application of the operator $n_{1/2,-1/2}$ gives rise to the structure MDO2′, in twin relation with MDO2).

The space group symmetry and the unit-cell parameters of the two MDO polytypes may be reliably derived as follows.

MDO1. The σ-operator $n_{1/2,2}$ normal to **a** is continuing in the succeeding layers, becoming a total glide [d – –] in a structure with $\mathbf{c} = 4\mathbf{c}_0$; the *C*-centering operator $\mathbf{a}/2 + \mathbf{b}/2$ is valid for all the layers and the σ-operators $n_{1/2,1/2}$ and $n_{1/2,-1/2}$ become total [– – d]

glides; the twofold axes parallel to **b** of the single layers (λ operators) are valid for the whole structure. Therefore, the MDO1 polytype is orthorhombic, with space group symmetry *Fd2d*, and unit-cell parameters $a = 11.310$, $b = 7.367$, $c = 54.274$ Å.

MDO2. The application of two successive operators $n_{1/2,1/2}$ (normal to **c**) corresponds to a translation $2\mathbf{c_0} + (\mathbf{a}+\mathbf{b})/2$. As all the layers are *C*-centered, the third layer is actually translated by $\mathbf{c} = 2\mathbf{c_0}$ relatively to the first one. Apart from the $(\mathbf{a}+\mathbf{b})/2$ translation, none of the λ- or σ-operators is valid for the whole structure. Therefore the MDO2 polytype is triclinic, with space-group symmetry *C*1 and unit-cell parameters $a = 11.310$, $b = 7.367$, $c = 27.137$ Å, $\alpha = 90°$, $\beta = 90°$, and $\gamma = 90°$. This cell could be transformed into a reduced primitive cell, but the *C*-centered one is preferred to make easier comparison with the MDO1 polytype and with the cell of the "family structure."

The silicate chains

Figure 7 shows all of the located sites associated with the silicate groups, with the likely Si-O bonds shown. The complex array of sites actually consists of two overlapping half-occupied wollastonite-like silicate chains. A similar situation has been described by Hoffmann and Armbruster (1997) in their refinement of the substructure of clinotobermorite. Other than the very long Si2-O4 bond, mentioned above, and the rather small O7-Si1b-O6b angle, 95.5°, the silicate groups have reasonable bond lengths and geometries (see Table 5). The chain is linked via the sequence -Si2-O6b-Si1b-O7-Si1a-O6a-Si2-. All of the O atoms that form the Si-O-Si links (O6a, O6b, and O7) are half-occupied, consistent with the fact that each of the overlapping chains is present only half of the time. Note that O6a is occupied when the adjacent Si1a site is occupied and the same is true for the O6b-Si1b pair. The O1, O2, O3, and O4 atoms form peripheral silicate vertices and all are fully occupied. Atoms O1 and O2 participate in both of the overlapping silicate chains and, therefore, are always silicate O atoms. On the other hand, O3 and O4 are only silicate O atoms half of the time. Both O3 and O4 are candidates for participating in a CO_3 group, but if they do not, O3 must be an OH and O4 must be an H_2O, based on bond-valence considerations (Table 6).

The O4 has significantly higher thermal displacement parameters (especially U_{11} and U_{22}) than any of the other O atoms. This may help to explain the very long Si2-O4 bond noted above. When the O4 is an H_2O and does not participate in the Si2 silicate group, it moves closer to Ca2; when it participates in the Si2 silicate group, it moves closer to Si2 and further from Ca2. As it stands, the bond-valence sum for O4 when it is bonded to Si2 is 0.80, but even with a normal Si2-O4 bond length, O4 would be significantly undersaturated in bond strength, suggesting that it has at least some OH (silanol) character when participating as part of the silicate chain. Nyfeler and Armbruster (1998) note that the Si-OH bond-length tends to be only modestly longer than the other Si-O bonds for silicate groups with two bridging O atoms (such as in whelanite), so this certainly does not explain the very long 1.84 Å bond length, but it is consistent with Si2-O4 being longer that the other Si-O bonds. For derivation of the ideal formula (see below), we assume that O4 has partial (½) OH character when participating in the silicate chain, i.e., ¼ OH character overall.

Where is the carbonate?

In spite of concerted efforts to locate and/or model the CO_3 group in the whelanite structure, no conclusive evidence for its placement was found. Existing O sites that could participate in a CO_3 group based upon bond-valence sums and geometric constraints are O3, O4, and O5. As noted above, O3 and O4 take part in the Si2 silicate group, but only half of the time. The other half of the time O3 must be either an OH group or a corner of the CO_3 group. If the latter is the case, and it has a normal bond length to C, it would be significantly oversaturated in bond strength (1.03 + 1.33 = 2.36 v.u.). When O4 is not bonded to Si2, it is either an H_2O group or a corner of the CO_3 group, but if the latter is the case, it would remain significantly undersaturated in bond strength (0.24 + 1.33 = 1.57 v.u.), unless it received multiple hydrogen bonds. The final possible participant in the CO_3 group is O5. From a bond-valence perspective, this presents the most attractive choice as it would be closer to bond-valence balanced (0.91 + 1.33 = 2.24 v.u.) and a somewhat longer than average C-O5 bond would improve matters. Furthermore, there appears to be plenty of space in the interlayer region adjacent to O5 to accommodate a CO_3 group. Examining residual electron density in the vicinities of the O3, O4, and O5 sites, indicates that significant residuals in the interlayer region are only present near the O5 site, including a 0.36 peak at [0.017, 0.500, 0.069] 1.24 Å from O5. Our attempt to refine this residual as a partially occupied C site were only marginally successful, in that no other sites could be located to successfully complete the CO_3 group. In the end, we are left to conclude that the CO_3 group is too disordered to be located using the existing structure data, but that its location in the interlayer region, bonded to O5, appears to be the most likely.

The ideal formula of whelanite

The original formula proposed for whelanite, $Cu_2Ca_5Si_6O_{17}(CO_3)(OH)_2{\cdot}4H_2O$, was based only on the chemical analyses. Although our structure determination failed to locate the CO_3 group, it does provide sufficient new information to better define the chemical formula. The total number of O sites provides 26 O apfu, and this is the basis we have used for calculating the empirical formula.

Using full Cu occupancy and ignoring C and H, the ideal formula thereby obtained is $[Cu_2Ca_6Si_6O_{26}]^{12-}$. Still neglecting C, bond-valence considerations indicate O5 to be OH, O3 to be ½ O and ½ OH, and O4 to be ¼ O, ¼ OH, and ½ H_2O (see above), yielding $[Cu_2Ca_6Si_6O_{17}(OH)_7(H_2O)_2]^{1-}$. Now the assumptions become more tenuous because of our failure to model the CO_3 group. Based upon the relatively low-electron density residuals, we prefer to assume that our structure refinement has accounted for all of the O atoms (26) and that any "additional" O atoms needed for the CO_3 group are balanced by small deficiencies in some of the located O sites. Furthermore, based upon the chemical analyses, we believe it best to use one CO_3 group pfu for the ideal formula. As a final assumption, we think it is most reasonable to replace a portion of the OH in the formula (corresponding principally with the O5 site) with CO_3. The resulting ideal formula for whelanite is $Cu_2Ca_6[Si_6O_{17}(OH)](CO_3)(OH)_3(H_2O)_2$, which is a reasonably good fit for the analyzed composition.

Related structures

As we have already noted, the calcium polyhedral layer in whelanite is very similar to that occurring in the minerals of the tobermorite group. The 9, 11, and 14 Å tobermorite structures (Merlino et al. 2000, 2001; Bonaccorsi et al. 2005) contain successively larger spacings between adjacent CaO_7 polyhedra layers. In tobermorite 11Å the wollastonite chains are connected to give double chains, whereas in tobermorite 9Å decondensation occurs and adjacent layers of Ca polyhedra approach each other. The tobermorite 14Å structure is the most similar to that of whelanite: both structures are characterized by the presence of single wollastonite chains of Si tetrahedra, which are connected on one side, by edge sharing, to the layer of CaO_7 polyhedra, and on the other side, by corner sharing, to octahedra in the interlayer region; however, whereas the interlayer region of tobermorite 14Å hosts columns of CaO_6 octahedra (Bonaccorsi et al. 2005), that of whelanite has a continuous brucite-like layer built up by columns of CaO_6 and CuO_6 octahedra.

The structures of dovyrenite (Kadiyski et al. 2008), roumaite (Biagioni et al. 2010), and rinkite (Cámara et al. 2011) all contain tobermorite-like layers of edge-sharing CaO_7 polyhedra, which alternate with modified brucite-like layers of edge-sharing octahedra, and have silicate linkages in between. However, these structures differ from that of whelanite in two important respects: (1) all three contain Si_2O_7 (disilicate) groups, rather than wollastonite-like chains, and (2) the tobermorite-like and brucite-like layers link directly to each other by corner-sharing.

The fukalite structure (Merlino et al. 2009) also exhibits some similarity to that of whelanite. Here, tobermorite-like layers alternate with tilleyite-like corrugated layers of edge-sharing six- and seven-coordinated Ca polyhedra. Between the layers are silicate chains, but not with a wollastonite-like configuration. Another intriguing similarity is the presence of a CO_3 group, which in fukalite shares an edge with the CaO_7 polyhedron of the tobermorite-like layer. This suggests the possibility that the unlocated CO_3 group in whelanite may assume a similar position; however, in whelanite the corresponding CaO_7 polyhedral edge is O1-O2, which is clearly part of the silicate chain.

Finally, it is worth noting that all of the aforementioned structures related to that of whelanite exhibit OD character.

Acknowledgments

Reviewers Fernando Cámara and Daniel Atencio and Associate Editor Fernando Colombo provided helpful comments on the manuscript. John Magnasco is thanked for information on the occurrences of whelanite, for his ongoing encouragement through the many often-frustrating years of this study and for providing specimens of whelanite from the Christmas mine and the Sunrise prospect. Sharon Cisneros is thanked for providing a specimen of whelanite from the Christmas mine. The late Fred Devito provided some specimens of the whelanite-like mineral (mineral Y) from Crestmore and later Thomas Loomis provided others from the Devito collection. Elena Sokolova is thanked for comments on some of the structural relationships. Frank Hawthorne, Peter Burns, Uwe Kolitsch, and Robert Downs are thanked for providing information regarding previous attempts to solve the whelanite structure. This study was funded by the John Jago Trelawney Endowment to the Mineral Sciences Department of the Natural History Museum of Los Angeles County.

References cited

Biagioni, C., Bonaccorsi, E., Merlino, S., Parodi, G.C., Perchiazzi, N., Chevrier, V., and Bersani, D. (2010) Roumaite, $(Ca,Na,\square)_3(Ca,REE,Na)_4(Nb,Ti)[Si_2O_7]_2(OH)F_3$, from Rouma Island, Los Archipelago, Guinea: a new mineral species related to dovyrenite. Canadian Mineralogist, 48, 17–28.

Bonaccorsi, E., Merlino, S., and Kampf, A.R. (2005) The crystal structure of tobermorite 14Å (plombierite), a C-S-H phase. Journal of the American Ceramic Society, 88, 505–512.

Brese, N.E. and O'Keeffe, M. (1991) Bond-valence parameters for solids. Acta Crystallographica B, 47, 192–197.

Brown, I.D. and Altermatt, D. (1985) Bond-valence parameters from a systematic analysis of the inorganic crystal structure database. Acta Crystallographica B, 41, 244–247.

Cámara, F., Sokolova, E., and Hawthorne, F.C. (2011) From structure topology to chemical composition. XII. Titanium silicates: the crystal chemistry of rinkite, Na_2Ca_4*REE*$Ti(Si_2O_7)_2OF_3$. Mineralogical Magazine, 75, 2755–2774.

Dornberger-Schiff, K. (1956) On the order-disorder structures (OD-structures). Acta Crystallographica, 9, 593–601.

——— (1964) Grundzüge einer Theorie von OD-Strukturen aus Schichten. Abhandlungen der Deutschen Akademie der Wissenschaften zu Berlin, Klasse für Chemie, Geologie und Biologie, 3, 1–107.

——— (1966) Lehrgang über OD-Strukturen. Akademie-Verlag, Berlin, 135 p.

Dornberger-Schiff, K. and Fichtner, K. (1972) On the symmetry of OD-structures consisting of equivalent layers. Kristall und Technik, 7, 1035–1056.

Ferraris, G., Makovicky, E., and Merlino, S. (2008) Crystallography of modular materials. IUCr Monographs on Crystallography, 15, Oxford University Press, New York, 372 p.

Flack, H.D. and Bernardinelli, G. (1999) Absolute structure and absolute configuration. Acta Crystallographica A, 55, 908–915.

Frost, R.L. and Xi, Y. (2012) Whelanite $Ca_5Cu_2(OH)_2CO_3Si_6O_{17}{\cdot}4H_2O$ – A vibrational spectroscopic study. Spectrochimica Acta Part A: Molecular and Biomolecular Spectroscopy, 91, 319–323.

Gunter, M.E., Bandli, B.R., Bloss, F.D., Evans, S.H., Su, S.C., and Weaver, R. (2004) Results from a McCrone spindle stage short course, a new version of EXCALIBR, and how to build a spindle stage. The Microscope, 52, 23–39.

Higashi, T. (2001) ABSCOR. Rigaku Corporation, Tokyo, Japan.

Hindman, J.R. (1976) Stringhamite, a new hydrous copper calcium silicate from Utah. American Mineralogist, 61, 189–192.

Hintze, L.F. and Whelan, J.A. (1973) Geology of the Milford area. Utah Geological Association, Publication 3.

Hoffmann, C. and Armbruster, T. (1997) Clinotobermorite $Ca_5[Si_3O_8(OH)_2{\cdot}4H_2O$–$Ca_5[Si_6O_{17}]{\cdot}5H_2O$, a natural C-S-H(I) cement mineral: determination of the substructure. Zeitschrift für Kristallographie, 212, 864–873.

Kadiyski, M., Armbruster, T., Galuskin, E.V., Pertsev, N.N., Zadov, A.E., Galuskina, I.O., Wrzalik, R., Dzierzanowski, P., and Kislov, E.V. (2008) The modular structure of dovyrenite, $Ca_6Zr[Si_2O_7]_2(OH)_4$: Alternate stacking of tobermorite and rosenbuschite-like units. American Mineralogist, 93, 456–462.

Mandarino, J.A. (1981) The Gladstone-Dale relationship: Part IV. The compatibility concept and its application. Canadian Mineralogist, 19, 441–450.

Merlino, S., Bonaccorsi, E., and Armbruster, T. (2000) The real structure of clinotobermorite and tobermorite 9Å: OD character, polytypes, and structural relationships. European Journal of Mineralogy, 12, 411–429.

——— (2001) The real structure of tobermorite 11Å: normal and anomalous forms, OD character and polytypic modifications. European Journal of Mineralogy, 13, 577–590.

Merlino, S., Bonaccorsi, E., Grabezhev, A.I., Zadov, A.E., Pertsev, N.N., and Chukanov, N.V. (2009) Fukalite: An example of an OD structure with two-dimensional disorder. American Mineralogist, 94, 323–333.

Morrison, S.M., Downs, R.T., and Yang, H. (2012) Redetermination of the kovdorskite, $Mg_2PO_4(OH){\cdot}3H_2O$. Acta Crystallographica Section E Structural Reports Online, 68, 12–13.

Murdoch, J. (1961) Crestmore, past and present. American Mineralogist, 46, 245–257.

Nyfeler, D. and Armbruster, T. (1998) Silanol groups in minerals and inorganic compounds. American Mineralogist, 83, 119–125.

Sheldrick, G.M. (2008) A short history of SHELX. Acta Crystallographica A, 64, 112–122.

Wray, W.B. (2006) Mines and geology of the Rocky and Beaver Lake districts, Beaver County, Utah. Utah Geological Association Publication 32, Mining Districts of Utah, 183–285.

Manuscript received March 28, 2012
Manuscript accepted July 9, 2012
Manuscript handled by Fernando Colombo